Hindawi
Journal of Nanomaterials
Volume 2020, Article ID 9450618, 15 pages
https://doi.org/10.1155/2020/9450618

Research Article

Codelivery of Emodin and Diammonium Glycyrrhizinate by Anti-alpha8 Integrin-Conjugated Immunoliposomes for the Treatment of Renal Fibrosis

Jiang Sun, Wenjie Yao, Xiaoting Luo, Zhishi Xu, and Yinghui Wei

College of Pharmaceutical Science, Zhejiang Chinese Medical University, Hangzhou 311402, China

Correspondence should be addressed to Yinghui Wei; yhw_nn@zcmu.edu.cn

Received 1 May 2020; Revised 20 July 2020; Accepted 29 July 2020; Published 28 August 2020

Academic Editor: Mohammad Rahimi-Gorji

The targeted delivery of therapeutics to the kidneys has a profound potential for the management of renal fibrosis. Thus, we developed a drug delivery system that targets mesangial cells by conjugating anti-alpha8 integrin to the surface of liposomes. We coloaded emodin (EMO) and diammonium glycyrrhizinate (DAG) to the immunoliposomes for combined therapy. The coloaded immunoliposomes were small size (92.4 ± 0.4 nm), narrowly distributed, and with nearly neutral zeta potential and good stability. The encapsulation rate of EMO and DAG in immunoliposomes was 45.5 ± 2.0% and 44.3 ± 1.1%, respectively. Using a BCA assay, the actual number of antibody molecules attached to a single liposome was determined as being approximately 41. An *in vitro* release study showed that EMO and DAG could be ratiometrically released from the immunoliposomes, which means that an optimized synergistic ratio of the two drugs could be achieved. Studies on cellular uptake studies demonstrated an approximately 3-fold increase for immunoliposomes in HBZY-1 cells compared to nonconjugated liposomes. *In vitro* cell growth inhibition and Western Blot assay revealed that the coloaded immunoliposomes exhibited a stronger and synergistic *in vitro* antifibrosis effect against NIH3T3 and HBZY-1 cells *in vitro*. Taken together, it indicated that anti-alpha8 integrin-modified immunoliposomes for codelivery of EMO and DAG have great potential for targeting the kidneys for the treatment of renal fibrosis.

1. Introduction

Renal fibrosis, which is the final common outcome of progressive kidney diseases, represents an attractive target for therapy in numerous chronic kidney diseases. More than 10% of the global population is affected by renal fibrosis [1, 2]. Renal fibrosis is characterized by the activation and proliferation of renal interstitial fibroblasts, excessive accumulation of extracellular matrix (ECM) in the renal stroma, and destruction of renal tissue [3, 4]. Numerous investigations have demonstrated that the development of renal fibrosis is closely associated with mesangial cells [5, 6]. Glomerular mesangial cells are involved in glomerular inflammatory response, repair of basement membrane, and the initiation of ECM overproduction, which are signs of progress of renal fibrosis. Phenotypic transformation of glomerular mesangial cells is activated after injury, followed by the production of several signaling molecules are produced such as transforming growth factor-β (TGF-β) and platelet-derived growth factor (PDGF), which contribute to excessive proliferation of mesangial cells and increases in matrix synthesis [7]. Mesangial cells (MCs) proliferation and extracellular matrix accumulation are also involved in the occurrence of glomerular inflammation and aggravate its progression to chronic diseases. Therefore, specific inhibition of mesangial cell activation and proliferation is of great significance in the treatment of renal fibrosis.

Alpha8 integrin, an RGD binding integrin, is a subtype of the integrin family and is expressed on mesangial cells. The alpha8 integrin chain combines with β1 integrin on mesangial cells to form the functional heterodimeric proteins.

These proteins play a critical role in cell proliferation, adhesion, differentiation, attachment, apoptosis, and phagocytosis, as well as in migration processes [8, 9]. Alpha8 integrin has already been proved to target therapeutic cargoes to mesangial cells. Thus, the treatment of renal fibrosis can be achieved by targeting mesangial cells mediated by anti-alpha8 integrin antibodies.

Clinically, angiotensin-converting enzyme inhibitors (ACEI), angiotensin receptor blockers (ARBs), and rennin inhibitors are recognized as first-choice medications for blocking the progression of renal fibrosis [10]. However, these therapeutic strategies are not effective enough in patients with middle or late stages of renal fibrosis. Moreover, hyperkalemia or even renal dysfunction caused by long-term application of ACEI/ARB is also the weakness of this therapeutic strategy. Furthermore, cytostatic and immunosuppressant drugs administered in clinics commonly produce severe side effects.

Nowadays, novel therapeutics and drug delivery systems have been proposed for slowing, arresting or even reversing, the progression of renal fibrosis including plant-derived active compounds [6]. Emodin (EMO) is an active anthraquinone present in the roots and barks of Chinese herbs, such as *Rheum palmatum* [11], *Polygonum cuspidatum* [12], and *Polygonum multiflorum* [13]. Investigations have shown that EMO ameliorates renal fibrosis in rats by reducing ECM synthesis by suppressing transforming growth factor-β1 (TGF-β1) and fibronectin (FN) overexpression [14], thus decreasing mRNA expression of TGF-β1 [15] and activating the PI3K/Akt/GSK-3β pathway [16]. EMO can also significantly inhibit the proliferation and hypertrophy of mesangial cells and extracellular matrix production. However, clinical trials have proven that EMO does not have insufficient quality and presents significant side effects especially when administered alone, due to its low water solubility and kidney nonspecificity [17], which prevent its use in patients. Diammonium glycyrrhizinate (DAG) is the diammonium salt of glycyrrhizin extracted from the root and rhizome of *Glycyrrhiza uralensis* Fisch [18], which has been reported as beneficial to renal fibrosis [19]. DAG can inhibit the expression of TGF-β1 and connective tissue growth factor (CTGF) in renal interstitial tissue [20], reduce the accumulation of extracellular matrix, alleviate the pathological damage to renal glomerulonephritis, and produce a positive effect on renal protection [21]. Hence, the combination of EMO and DAG can act on renal fibrosis by utilizing multiple nonoverlapping and synergistic mechanisms, thus improving antifibrosis activity. We explored the cell growth inhibition of EMO and DAG in NIH3T3 cells in a previous study. Results showed that the combined use of EMO and DAG could exert a synergistic effect when the mole ratio between EMO and DAG changed from 1 : 2 to 1 : 10 (Figures S1 and S2). Moreover, renal fibrosis-associated protein expression including α-SMA, TGF-β1, Col-I, and FN expression was significantly decreased (Figures S3 and S4). Nevertheless, the traditional combination cannot effectively control the dosage regimen and effective drug ratio at the target tissue, which is caused by different physicochemical properties and pharmacokinetics of individual drugs [22]. A promising strategy for addressing these drawbacks is the use of nanosized delivery platforms. Moreover, nanosized delivery platforms, such as liposomes and polymeric nanoparticles, are important targeting strategies to mesangial cells [23]. Thus, liposomes may be an appropriate delivery system for codelivery of EMO and DAG in renal fibrosis, and it can encapsulate both hydrophilic (DAG) and hydrophobic drugs (EMO) based on the amphiphilic properties of phospholipids and guarantee the optimized synergistic effect of DAG and EMO. To date, liposomes have gained momentum in the research of drug delivery with advantages such as improved drug efficacy, low toxicity, and enhanced pharmacokinetics and stability [24]. Significantly, liposomes (LPs) can be conjugated to antibodies on their surface to form immunoliposomes (ILPs). ILPs modified by Thy1.1 antibody or anti-α8 integrin have been used mainly for targeting to mesangial cells. Moreover, ILPs modified with anti-α8 integrin have higher translational potential in humans [23].

The purpose of this investigation is to develop coloaded anti-alpha8 integrin-modified EMO/DAG-ILPs and to evaluate their cell binding and uptake properties by HBZY-1 (alpha8 integrin receptor positively expressed cells) and HK-2 cells (alpha8 integrin receptor negatively expressed cells). Furthermore, the NIH3T3 cell line, which was widely used in the study of renal fibrosis as an *in vitro* model of fibrosis [25–27], was chosen to evaluate the antifibrotic effects and mechanism of EMO/DAG-loaded ILPs, cell growth inhibition, and levels of fibrosis protein expression.

2. Materials and Methods

2.1. Materials. Diammonium glycyrrhizinate (purity ≥ 97%) and emodin (purity ≥ 98%) were purchased from Xi'an Fujie Pharmaceutical Co., Ltd. (Xi'an, China) and Nanjing Zelang Pharmaceutical Co., Ltd. (Nanjing, China), respectively. 1,2-distearoyl-sn-glycero-3-phosphocholine (DSPC), 1,2-disearoyl-sn-glycero-3-phosphoethanolamine-N-[methoxy(polyethylene glycol)-2000](DSPE-PEG2000), 1,2-distearoyl-sn-glycero-3-phosphoethanolamine-N-[maleimide(polyethylene glycol)-2000] (DSPE-PEG2000-MAL), and cholesterol (CHOL) were obtained from Avanti Polar Lipids (Alabaster, AL, USA). Stearylamine (SA, ≥96%) was purchased from Shanghai Hengyuan Biotechnology Co., Ltd. (Shanghai, China). (3-(4,5-Dimethylthiazol-2-yl)-2,5-Diphenyltetrazolium bromide) and dimethyl sulfoxide (DMSO) were purchased from Sigma-Aldrich (St. Louis, MO, USA). Dulbecco's modified Eagle's medium (DMEM), fetal bovine serum (FBS), trypsin-EDTA (0.05%), and penicillin/streptomycin were purchased from Gibco BRL (Gaithersberg, USA). Primary antibodies such as Smad3 IgG, α-SMA IgG, Col1 IgG, and FN IgG were obtained from Abcam Corporation (Shanghai, China). Goat anti-rabbit IgG was purchased from LI-COR Biosciences (USA). Anti-alpha8 integrin was purchased from Shanghai Leuven Biotechnology Co., Ltd. (Shanghai, China). BCA kit and RIPA Lysis Buffer were obtained from Beyotime Institute of Biotechnology (Shanghai, China). 1,1′-Dioctadecyl-3,3,3′,3′-tetramethylindocarbocyanine perchlorate (DiI, ≥98%) was purchased from Shanghai Yi Sheng Biotechnology Co., Ltd. (Shanghai, China). Transforming growth factor-β1 (TGF-β1) was purchased from Peprotech Corporation (USA).

2.2. Cell Culture. Murine fibroblast (NIH3T3) cell line, rat glomerular mesangial cell line (HBZY-1 cells), and human kidney-2 cells (HK-2 cells) were obtained from Chinese Academy of Medical Sciences (Shanghai, China) and cultured in Dulbecco's modified Eagle's medium (DMEM), supplemented with 10% (*v*/*v*) fetal bovine serum, penicillin (100 units/mL), and streptomycin (0.1 mg/mL) in a humidified incubator at 37°C with 5% CO_2.

2.3. Preparation of EMO/DAG-Loaded Long-Circulating Liposomes. The EMO/DAG-loaded long-circulating liposomes (EMO/DAG-LPs) were prepared using ethanol injection and followed by application of the calcium acetate gradient method. Briefly, DSPC, CHOL, DSPE-PEG2000, SA, and EMO were dissolved in 1 mL of alcohol at a molar ratio of 47 : 36 : 1 : 7 : 6. This solution was added dropwise into 10 mL of 0.12 mmol/L calcium acetate solution maintained at 65°C and stirred for 30 min, resulting in EMO-loaded liposomes (EMO-LPs). Then, the DAG solution (10 mg/mL) was added to the preformed EMO-LPs and incubated at 60°C for 30 min to obtain EMO/DAG-LPs, which were then cooled down to room temperature. The liposomes were successively extruded 3 times through 200 nm and 100 nm polycarbonate membranes using an extruder (HOMOEX-25, HOMOEX, Shanghai, China). Unentrapped drugs and calcium acetate were removed from liposomes by dialyzing liposomes in 600 mL of 0.9% sodium chloride solution.

2.4. Preparation of EMO/DAG-Loaded ILPs. The functionalization of liposomes with anti-alpha8 integrin was performed using a modified postinsertion method [28, 29]. First, anti-alpha8 integrin was dissolved in HEPES buffer (pH 8.0) containing 2 mM EDTA and then thiolated with Traut's reagent at a molar ratio of 1 : 50, followed by incubation for 1 h at room temperature. The unreacted Traut's reagent was then removed from a HiTrap desalting column eluted with HEPES buffer (pH 7.4). Subsequently, the obtained thiolated monoclonal antibody (mAbs) was directly mixed with DSPE-PEG2000-Mal at a molar ratio of 1 : 100, shaken well and incubated for 12 h at 4°C. Then, EMO/DAG-loaded ILPs (EMO/DAG-ILPs) with anti-alpha8 integrin to lipids at a molar ratio of 1 : 250 were then prepared by mixing the resultant DSPE-PEG2000-Mal-mAbs with preformed liposomes and incubating them for 24 h at 4°C with continuous and gentle shaking. Final formulations were purified on a Sepharose CL-4B column with HEPES buffer (pH 7.4) as the eluent and then stored at 4°C until used. The ILPs containing DiI were prepared according to the above-mentioned method under dark conditions.

2.5. Characterization of Liposomal Samples. Particle size distribution, polydispersity index (PDI), and zeta potential of LPs and ILPs were measured at 25°C using a dynamic light scattering (DLS) and the laser Doppler electrophoresis system (ZEN 3690, Malvern, Worcestershire, UK). Samples were diluted in distilled deionized water and then dropped on the surface of a copper grid and air dried in order to observe the morphology of liposomes. The grid was observed using transmission electron microscopy after staining with 2.0% phosphotungstic acid hydrate (H-7650, Hitachi, Japan).

Entrapment efficiency (EE%) in liposomal formulations was determined using the ultrafiltration centrifugation method. To achieve this, 1 mL of liposomal formulations was added into an ultrafiltration centrifuge tube (MWCO, 30 kDa, Millipore, USA) and centrifuged for 10 min at 10000 r/min. The amounts of EMO and DAG in the filtrate were analyzed using a valid HPLC method. The total liposome fraction was also disrupted and solubilized in menthol. The samples were then diluted, sonicated, and analyzed in triplicate using the same HPLC method mentioned above. The C18 column (Ultimate XB-C18, 5 μm, 4.6 × 250 mm, Welch Inc., USA) was used for HPLC analysis. The mobile phase consisted of acetonitrile and 0.2% phosphoric acid, and the UV detection wavelength was 250 nm.

EE% was calculated according to the following equation:

$$\mathrm{EE}(\%) = \frac{W_{\mathrm{total}} - W_{\mathrm{unencapsulated}}}{W_{\mathrm{total}}} \times 100\%, \quad (1)$$

where W_{total} means the amount of drug in the total fraction and $W_{\mathrm{unencapsulated}}$ means the weight of unencapsulated drug.

2.6. Antibody Conjugation Efficiency in ILPs. The conjugation efficiency of anti-alpha8 integrin coupled to the surface of liposomes was determined though BCA protein assay, described as follows [30]. Briefly, the BCA working reagent was configured by mixing reagent A with the reagent B at a volume of 50 : 1. Then, 20 μL of each protein standard sample was added into 96-well plates, followed by adding 200 μL of working reagent and incubated at 37°C for 30 min. Subsequently, absorbance was measured at 562 nm using a microplate reader (SpectraMax M2, Molecular Devices, USA). The number of conjugated antibodies on the surface of the ILPs was calculated considering the following assumptions: (i) the liposome was unilamellar; (ii) the number of phospholipid molecules per liposome was approximately 80000 [31]; and (iii) the molecular mass of anti-alpha8 integrin was 117KDa [32]. Antibody conjugation efficiency and number of antibodies on the ILPs were calculated using equations as follows:

$$\begin{aligned}
\text{Conjugation efficiency } (\%) &= \frac{\text{the amount of mAbs in immnolipsomes}}{\text{the total mAbs employed for conjugation}} \times 100\%, \\
\text{Number of antibodies on the immunoliposomes} &= \frac{W_{\mathrm{mAbs}}}{MW_{\mathrm{mAbs}} \times M_{\mathrm{DSPC}}} \times 80000,
\end{aligned} \quad (2)$$

where W_{mAbs} means the weight of anti-alpha8 integrin in ILPs, MW_{mAbs} means the molecular mass of anti-alpha8 integrin, and M_{DSPC} means the amount of substance of DSPC.

2.7. Stability of the ILPs. ILPs were blended into FBS (1 : 1, *v* : *v*) and incubated with shaking at 37°C for this evaluation. The samples were withdrawn at predefined time intervals (1, 2, 4, 6, 8, 10, 12, 24, and 48 h). ILP serum stability was determined by measuring particle size, PDI, and zeta potential.

2.8. In Vitro Drug Release. The *in vitro* release behavior of EMO and DAG from the liposomes (EMO/DAG-LPs and EMO/DAG-ILPs) was evaluated according to the dialysis method in phosphate buffer solution (PBS, pH 7.4) containing 20% ethanol for 48 h. Briefly, 5 mL of formulation equivalent to 0.42 mg EMO and 5.46 mg DAG was sealed in a dialysis bag (MWCO 3500) and immersed into 200 mL of release medium with continuous stirring at 37°C. At prearranged time intervals, 1 mL of the solution was withdrawn and replaced with the same volume of fresh medium. The collected samples were filtered with 0.22 mm filters, and the amounts of EMO and DAG were determined using the HPLC method.

Furthermore, to evaluate the influence of plasma on release behavior, the liposomal formulation was mixed with plasma, which was diluted twice with phosphate buffer solution (PBS, pH 7.4), at a final concentration of 0.11 mg/mL for EMO and 1.39 mg/mL for DAG, sealed in a dialysis bag, and then suspended in 200 mL of phosphate buffer solution (PBS, pH 7.4) containing 20% ethanol. All experiments were carried out in triplicate.

2.9. In Vitro Cell Delivery and Uptake of ILPs. Studies on specific binding and uptake of liposomes and ILPs were performed by incubating HBZY-1 and HK-2 cells with DiI-labeled liposomal samples, which were prepared using fluorescent DiI at 16 μmol as of lipid bilayers. Cellular delivery of the liposomal samples was monitored using confocal laser scanning microscopy (CLSM). To achieve this, HBZY-1 cells and HK-2 cells were seeded onto 4-well plates at a density of 5×10^5 cells/well and incubated at 37°C overnight, respectively. After washing twice with phosphate buffer solution (PBS, pH 7.4), the cells were incubated with DiI-labeled liposomes (DiI-LPs) or DiI-labeled immunoliposomes (DiI-ILPs) at 37°C for 2, 4, or 6 h, respectively. The cells were then rinsed and fixed with 4% (*v*/*v*) formaldehyde for 10 min in a darkroom. Finally, the cells were further rinsed, stained with Hoechst 33342 (12 μg/mL) for 10 min, and then visualized using a confocal laser scanning microscope (Zeiss LSM510, Carl Zeiss, Germany).

To further quantify the cellular uptake, HBZY-1 and HK-2 cells were seeded onto 6-well plates at a density of 5×10^5 cells/well and incubated at 37°C overnight, respectively. After incubation with DiI-LPs or DiI-ILPs for 4 h, the cells were harvested, trypsinized, and washed with 4°C phosphate buffer solution (PBS, pH 7.4), and finally the fluorescence intensity was analyzed by flow cytometry (Guava easyCyte 12HT, Merck Millipore, Germany).

2.10. In Vitro Cell Growth Inhibition Assay. The inhibition effect of different formulations on cell growth was investigated in both NIH3T3 and HBZY-1 cells through MTT assays. In this study, the cells were seeded in 96-well plates at a density of 2×10^4 cells/well and incubated for 24 h at 37°C. Then, the culture medium was discarded, and the cells were washed with phosphate buffer solution (PBS, pH 7.4) before the different drug-loaded formulations or blank ILPs were added. After incubation for 48 h, 20 μL of MTT (5 mg/mL) solution was added to each well and incubated for another 4 h at 37°C. Subsequently, the supernatant solution containing MTT was carefully removed, and the formazan salt that formed was dissolved in 150 μL of DMSO. Absorbance was measured in each well at a wavelength of 570 nm using a microplate reader (SpectraMax M2, Molecular Devices, USA). Percentage growth (%) was calculated according to the following equation:

$$\text{Cell viability}\,(\%) = \frac{OD_{570(\text{sample})} - OD_{570(\text{blank})}}{OD_{570(\text{control})} - OD_{570(\text{blank})}} \times 100\%, \tag{3}$$

where $OD_{570(\text{sample})}$ was the absorbance of cells incubated with various formulations, $OD_{570(\text{control})}$ was the absorbance of cells treated with fresh cellular culture medium, and $OD_{570(\text{blank})}$ was the absorbance of culture medium without cells. The mean drug concentration required for 50% growth inhibition (IC_{50}) was calculated by the nonlinear regression equation by using the SPSS Statistics 22.0 software. Each concentration was tested in five wells, and data was presented as mean ± standard deviation (SD).

2.11. Western Blot Analysis. The antifibrotic effects of ILPs were investigated using Western Blotting by observing the expression of fibrosis protein (α-SMA, Col-I, FN, and Smad3). NIH3T3 cells and HBZY-1 cells were plated into 6-well plates at a density of 1.5×10^4 cells/well. After incubation overnight, the cells were treated with 5 ng/mL of TGF-β1 and incubated for 48 h [33]. The cell culture medium was then substituted with different formulations (EMO solution, DAG solution, EMO/DAG solution, EMO/DAG-LPs, and EMO/DAG-ILPs) and incubated at 37°C for 24 h. As a control for the profibrotic effect of TGF-β1, cells were cultured in medium alone (without TGF-β1 or any formulations). The cells were then harvested and lysed using RIPA buffer, and the supernatants were collected after centrifugation (12000 rpm at 4°C for 10 min). The protein concentration of each sample was determined using a BCA protein quantitative kit. Aliquots corresponding to 30 μg of the protein were separated on 8% SDS-PAGE gel for 1 h, followed by transfer onto the PVDF membranes for 1.5 h. The membranes were blocked with 5% skimmed milk for 1 h followed by overnight incubation at 4°C with diluted primary antibodies against α-SMA (1 : 500, Abcam, USA), Smad3 (1 : 500, Abcam, USA), Col-I (1 : 1000, Abcam, USA), FN (1 : 1000, Abcam, USA), and GAPDH (1 : 1000, Abcam, USA) antibodies and were used as the internal loading control. The membranes were incubated with a secondary antibody (goat anti-rabbit IgG) at room temperature for 1 h after three washings. Finally, protein bands were detected using the LI-COR/Odyssey infrared image system (LI-COR Bioscience, Lincoln, NE) for capturing images.

2.12. Statistical Analysis. Data were presented as mean ± SD. The statistical significant analysis was performed using Student's *t*-test through SPSS 21.0, and a *P* value less than 0.05 was considered statistically significant.

3. Results and Discussion

3.1. Preparation and Characterization of ILPs. The morphology of liposomal formulations appeared as spherical unilamellar structures with good dispersity as shown in Figure 1. The physicochemical properties of LPs and ILPs are shown in Table 1. Particle sizes of LPs and ILPs were 86.2 ± 1.1 nm and 92.4 ± 0.4 nm in diameter, respectively, indicating that surface modification of liposomes with anti-alpha8 integrin did not show any significant difference ($P > 0.05$) in particle sizes. All liposomal formulations show homogeneous dispersibility with a PDI of <0.2. The zeta potentials of LPs and ILPs were comparable and were 5.6 ± 0.4 mV and 4.3 ± 0.2 mV, respectively. Additionally, in this investigation, thiolated anti-alpha8 integrin was successfully conjugated to the DSPE-PEG2000-MAL present on the surface of liposomes with a conjugation efficiency of 60.8 ± 2.0%, corresponding to approximately 41 anti-alpha8 integrin molecules per liposome. It turned out that prepared ILPs are sufficient to achieve an efficient targeting effect, which is consistent with previous reports that at least 10-20 ligands/liposomes are sufficient to perform selective targeting delivery [34, 35].

EMO was entrapped into liposomes according to the ethanol injection method with EE% of 46.7 ± 1.1% and 45.5 ± 2.0% for EMO/DAG-LPs and EMO/DAG-ILPs, respectively, as shown in Table 1. The relatively low entrapment efficiency of EMO is due to the application of stearylamine cationic agent in the preparation. The existence of a charged interface leads to a decrease in the volume of the lipid bimolecular layer [36]. Considering its strong hydrophilicity (log $P = -2.89$), DAG was actively loaded into the liposomal formulations according to the calcium acetate gradient method to increase its EE%. The method resulted in an EE% of DAG of 58.2 ± 5.0% in liposomes. Nevertheless, the EE% of DAG in ILPs decreased by approximately 14% compared to the LPs, which was only about 44.3 ± 1.1% and may be due to the modification process. Similar results reported by Manjappa et al. [37], Devi et al. [38], and Peres-Filho et al. [39] showed that the encapsulation efficiency of cargoes in liposomal formulations was reduced by 5%, 10%-12%, and 16%, respectively, after modification with anti-neuropilin-1, lactic acid, and folic acid, respectively. Furthermore, the determined loading molar ratio between EMO and DAG was 1 : 3.7 and 1 : 2.7 in the prepared LPs and ILPs, respectively, which was consistent with the designed radiometric of EMO and DAG for synergistic effects (Figures S1 and S2). The final EMO and DAG concentrations in immunoliposomes were 0.08 mg/mL and 0.49 mg/mL, respectively.

As shown in Figure 2(a), no significant changes in particle size and PDI of ILPs were observed after incubation with 10% FBS for 12 h. Moreover, the zeta potential of ILPs hardly changed over 12 h (Figure 2(b)). Thus, both the LPs and ILPs were stable in serum despite of the low zeta potential value, which might be due to the PEG surface modification. Many studies have proved that nanoparticles stability not only depends on the repulsive electrostatic double layer (zeta potential value) but also is closely related to the van der Waals and structural forces (surface functionalization) [40–42]. Surface functionalization can reduce the probability of nanostructure aggregation, prevent the nonspecific adsorption, and increase the steric stability of liposomes [42–44]. For instance, Smith et al. found that PEG modification greatly improved the stability of DOTAP liposomes and DOP liposomes [45].

3.2. In Vitro Drug Release. The *in vitro* release profiles of EMO and DAG from liposomal formulations in release medium over the period of 72 h are shown in Figure 3. It is obvious that the release behavior of EMO and DAG from LPs and ILPs are similar, demonstrating that antibody modification does not affect drug release, which is consistent with previous research [46]. The limited ability of the phospholipid bilayer membrane to retain hydrophilic drugs led to higher release of DAG compared to EMO, which was 93.7% from the LPs and 91.3% from the ILPs, while the cumulative release of EMO from the LPs and ILPs was 75.8% and 71.6%, respectively. The release pattern of DAG could be divided into two stages, including initial burst release followed by sustained release. More than 20% of the drug was released within 2 h followed by an additional 70% release within 72 h. Moreover, although the molar ratio of EMO/DAG released from both LPs and ILPS exceeded 1 : 10 within the initial 2 h due to the burst release of DAG, both the LPs and ILPs can better control the molar ratio of EMO/DAG around 1 : 5 after 4 h, which is in accordance with the optimized synergistic effect.

Addition of plasma to the LPs and ILPs did not cause obvious aggregation within the dialysis bag for the duration of 72 h, neither was any noticeable change observed in the DAG release behavior. However, the presence of plasma significantly delayed the release of EMO from the LPs and ILPs, which was only approximately 41.8% and 45.5%, respectively, as illustrated in Figure 3(b). This may due to the high protein-binding efficiency of EMO, which is up to 99.6% [47].

3.3. Cellular Uptake and Intracellular Disposition. To evaluate the intracellular disposition and uptake behavior of ILPs, both alpha8 integrin receptor positively expressed cell line, HBZY-1, and negatively expressed HK-2 cell line were used in this study. As shown in Figure 4(a), fluorescence intensity is boosted up with the increase of incubation time, demonstrating that liposomes have ability to deliver different formulations to these two cell lines. Furthermore, the fluorescence intensity of ILPs was significantly stronger in the HBZY-1 cell line than in that of the LPs, indicating enhanced uptake, possibly mediated by endocytosis through anti-alpha8 integrin and alpha8 integrin receptor interaction., No remarkable difference was seen between the LPs and ILPs in HK-2 cells. This result is consistent with previous studies, which reported that high expression of alpha8 integrin facilitated phagocytosis by renal mesangial cells [8].

Flow cytometry analysis was conducted to further quantify intracellular uptake by HK-2 and HBZY-1 cells. As shown in Figure 4(c), there was no difference in mean fluorescence intensity for all liposomal groups in HK-2 cell lines after 4 h of coincubation, indicating that neither DiI-ILPs nor DiI-LPs barely bind to HK-2 cell lines. On the other hand, the mean fluorescence intensity of DiI-ILPs increased significantly compared to that of the DiI-LPs group in

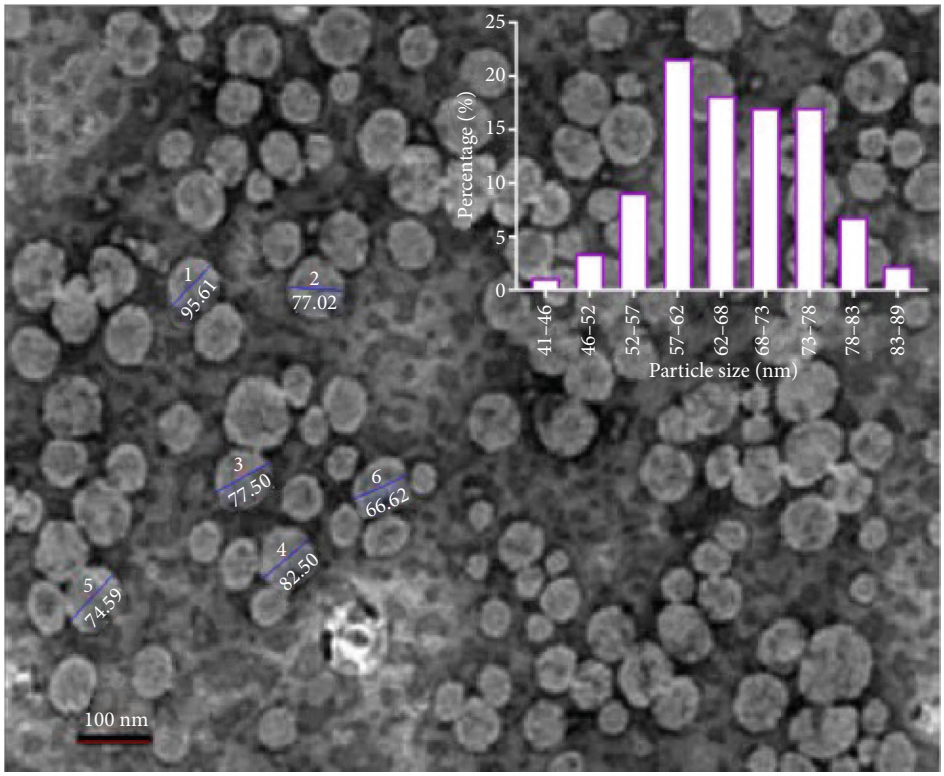

(a)

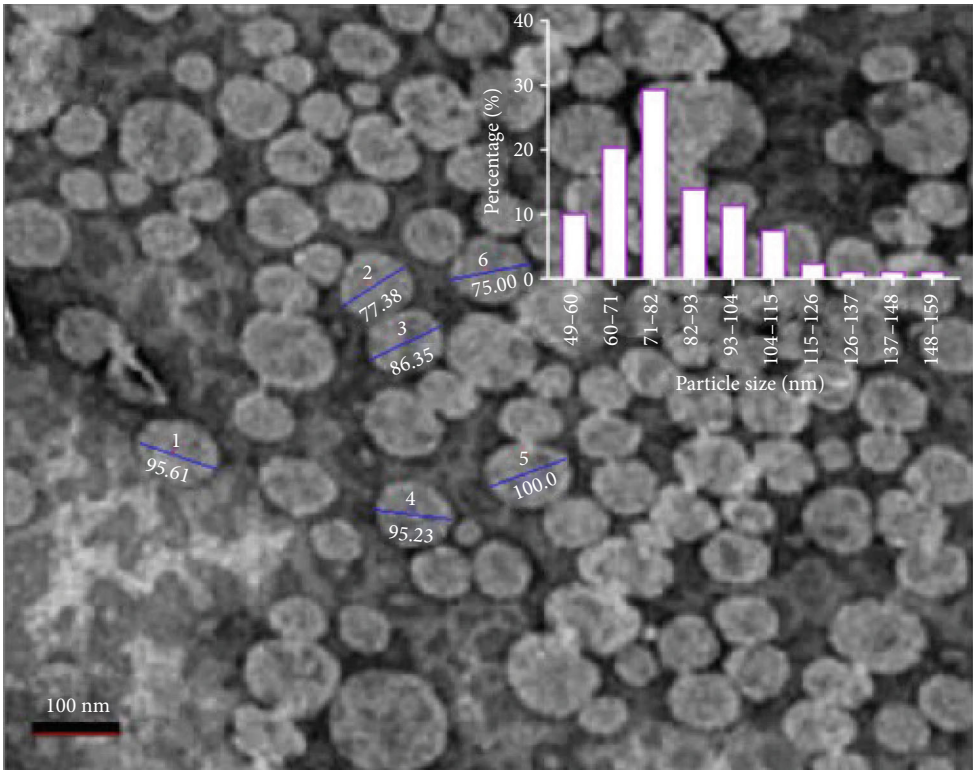

(b)

Figure 1: The morphology of LPs (a) and ILPs (b) by TEM.

Table 1: Characterization of liposomal formulations[a].

Formula	Size (nm)	PDI	Zeta potential (mV)	EE (%)	
				EMO	DAG
LPs	86.2 ± 1.1	0.15 ± 0.01	5.6 ± 0.4	46.7 ± 1.1	58.2 ± 5.0
ILPs	92.4 ± 0.4	0.15 ± 0.02	4.3 ± 0.2	45.5 ± 2.0	44.3 ± 1.1

[a]Data represented as means ± SD and was measured in triplicate.

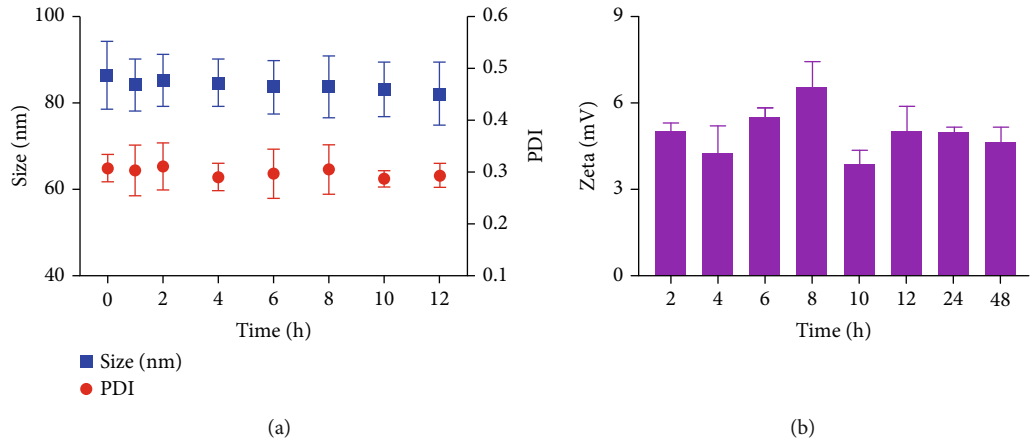

Figure 2: Serum stability of ILPs. Scatter graph represents particle size and PDI (a), and histogram represents zeta potential (b).

HBZY-1 cells ($P < 0.01$), suggesting that anti-alpha8 integrin fragments conjugated to the surface of liposomes were reactive, thus facilitating the binding of ILPs to alpha8 integrin-overexpressed cells (i.e., HBZY-1 cells) specifically, as shown in Figures 4(b) and 4(d). The cellular uptake rate of ILPs by HBZY-1 cells was approximate 3-folds as high as that of the LPs ($P < 0.01$). These results further confirmed the effectiveness of anti-alpha8 integrin-modified ILPs in the cellular uptake of HBZY-1 cells, which is in consistent with the findings of Scindia et al. [48], who constructed anti-alpha8 integrin-modified ILPs and demonstrated that mesangial cell-targeted delivery by anti-alpha8 integrin ILs opens up a novel method for treating glomerular diseases.

3.4. In Vitro Cell Growth Inhibition Activity of ILPs. *In vitro* biocompatibility of blank liposomal formulations was first evaluated using the MTT assay in NIH3T3 and HBZY-1 cells. As illustrated in Figures 5(a) and 5(c), cell viabilities were more than 85% after exposure to blank liposomal formulations at a phospholipid concentration range of 0.037 to 1.184 mM. This result showed that blank liposomes, whether they were modified with anti-alpha8 integrin or not, exhibited low cytotoxicity and high biocompatibility on HBZY-1 cells and NIH3T3 cells. The MTT assay was conducted using different formulations to compare the inhibitory effect of EMO and DAG in solutions and in liposomal formulations. As shown by a higher proportion of inhibited cells (Figures 5(b) and 5(d)) and lower IC_{50} values (Table 2), EMO and DAG combined treatment, whether in solutions or in liposomal formulations, showed an explicit enhanced inhibition effect in both NIH3T3 and HBZY-1 cells compared to individual treatments ($P < 0.05$). Furthermore, EMO/DAG-LPs and EMO/DAG-ILPs inhibited the growth of NIH3T3 cells more significantly than EMO/DAG solution ($P < 0.01$). This could be attributed to the enhancement of cellular uptake and effective delivering capability of liposomal formulations. However, compared to EMO/DAG-LPs, EMO/DAG-ILPs conjugated with anti-alpha8 integrin antibody did not show a significant decrease in cell viability in NIH3T3 cell lines, which does not express alpha8 integrin receptor. On the other hand, EMO/DAG-ILPs had reduced IC_{50} values in HBZY-1 cells compared to the EMO/DAG-LPs, which was expected and was consistent with the cellular uptake finding, indicating that the EMO/DAG-ILPs were endocytosed via the alpha8 integrin receptor-mediated pathway. We also found that, compared to NIH3T3 cells, HBZY-1 cells are more sensitive to EMO/DAG-ILPs ($P < 0.05$), which might be due to the expression of alpha8 integrin receptors. Thus, we hypothesized that ILPs could weaken the transdifferentiation of MCs into fibroblasts. These findings imply that ILPs treat renal fibrosis by inhibiting the proliferation of MCs and attenuating the transformation of MCs into fibroblasts.

3.5. Regulating Effects on Renal Fibrosis-Related Proteins. It is well known that TGF-β1 is a crucial pathological factor in promoting renal fibrosis which can directly induce the production of ECM, including collagen I (Col-I), and fibronectin (FN). TGF-β1 can also act directly on various kidney cells, such as promoting mesangial cell proliferation [49]. In addition, numbers of studies have identified Smad3 as major signaling mediators downstream of the TGF-β1 signal and have substantiated that the development of renal fibrosis is positively correlated with Smad3 [50]. α-SMA is the hallmark protein of myofibroblasts, which plays an important role in renal fibrosis, such as accelerating fibrous tissue contraction

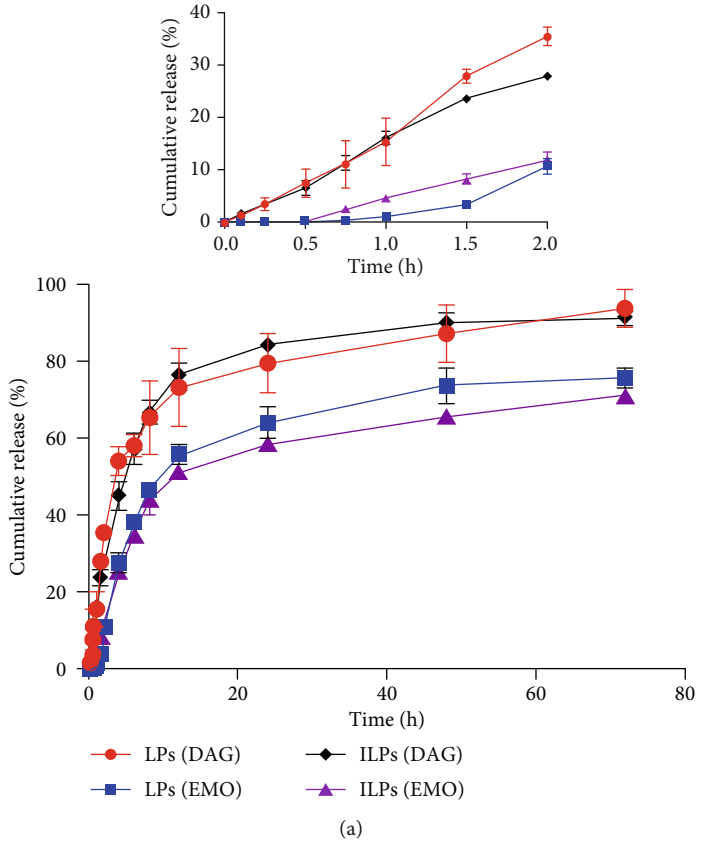

(a)

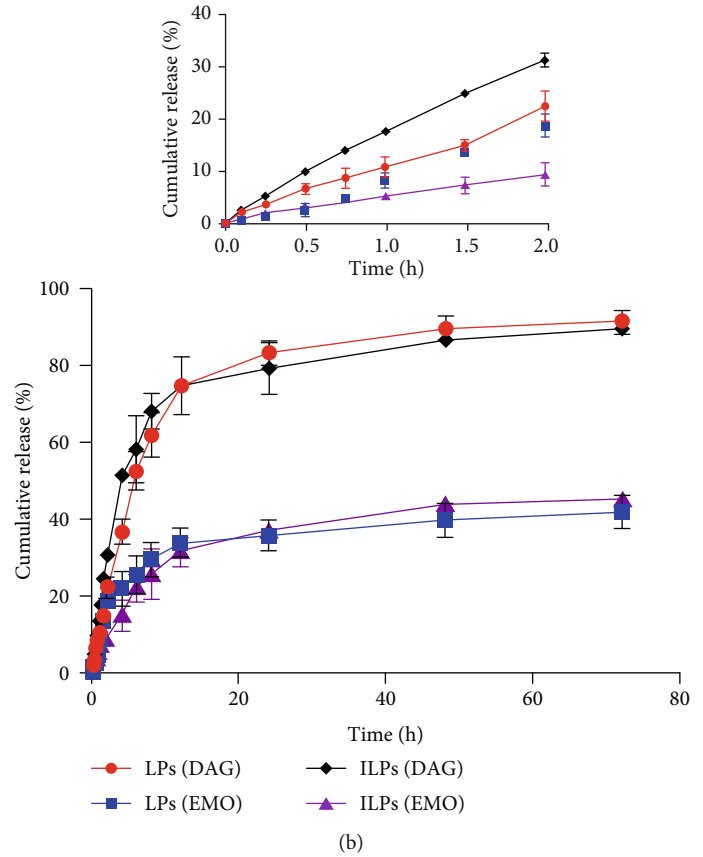

(b)

Figure 3: *In vitro* release of EMO and DAG from liposomal formulations in phosphate buffer solution (PBS, pH 7.4) (a) and in the presence of plasma (pH 7.4) (b) ($n = 3$).

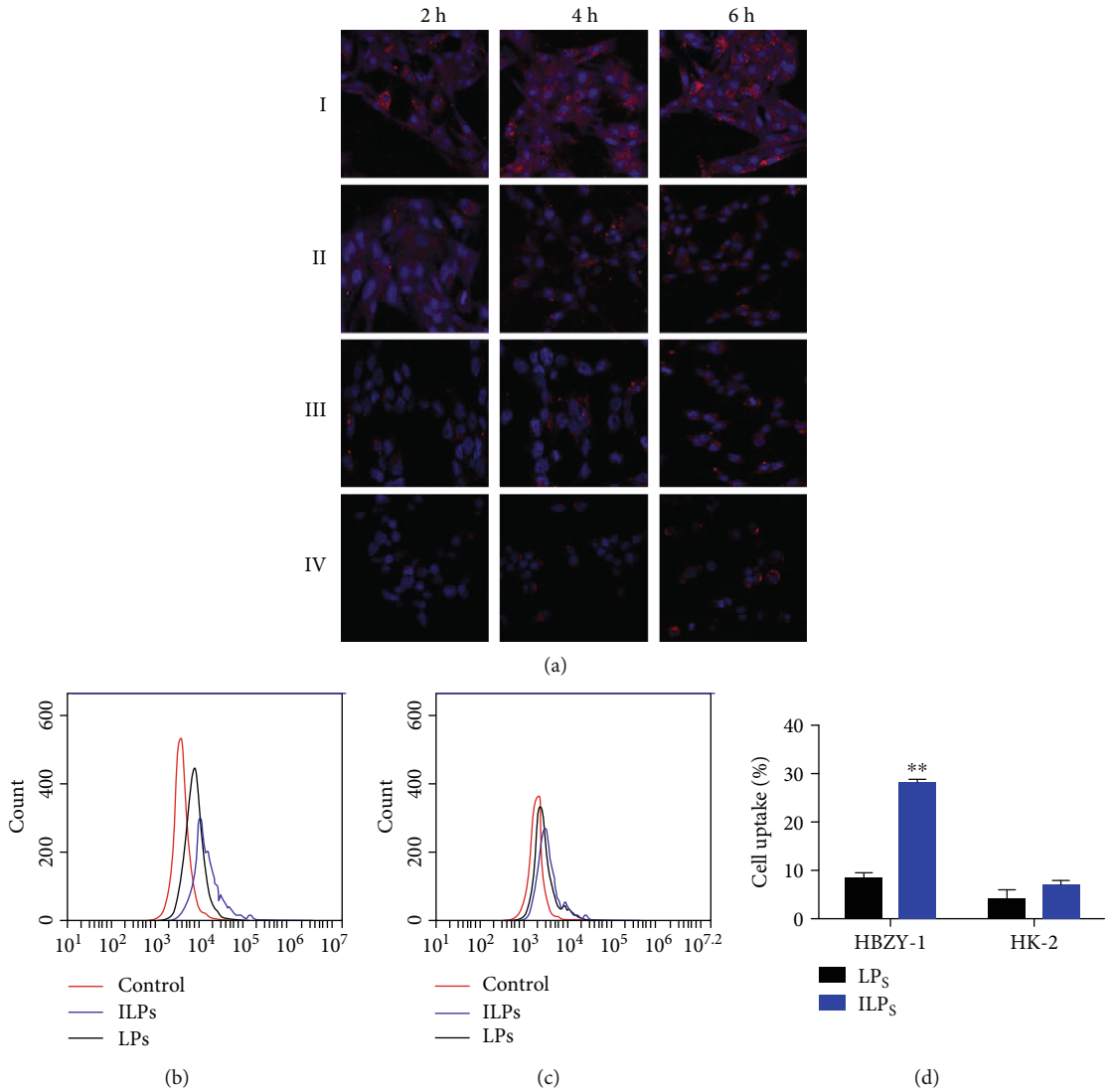

Figure 4: Intracellular uptake of DiI-labeled liposomal formulations in HBZY-1 cells and HK-2 cells. CLSM images for HBZY-1 cells and HK-2 cells (a). I, vs. DiI-ILPs in HBZY-1 cells; II, vs. DiI-LPs in HBZY-1 cells; III, vs. DiI-ILPs in HK-2 cells; IV, vs. DiI-LPs in HK-2 cells. Graphic demonstration of FCM analysis of HBZY-1 cells (b) and HK-2 cells (c) after 4 h-incubation. (d) Quantitative FCM histogram ($*P < 0.05$, $**P < 0.01$, compared to the LPs group).

and aggravating the hypoxia of renal tissue. α-SMA levels are positively correlated with the degree of renal interstitial fibrosis and the level of renal function. Thus, Col-I, FN, Smad3, and α-SMA were chosen to estimate the effects of EMO/-DAG-ILPs on renal fibrosis through Western Blot assay. In this investigation, NIH3T3 cells were simulated by TGF-β1 (5 ng/mL), and the renal fibrosis-related protein expression was explored after treatment with EMO/DAG-ILPs. As shown in Figure 6, the protein levels of Smad3, α-SMA, Col-I, and FN in the model group were significantly elevated after stimulation with TGF-β1 compared to the control group. After treatment with different formulations, the protein levels of Smad3, α-SMA, Col-I, and FN were significantly reduced except for the DAG group. This result suggested that both free EMO and the combination of EMO and DAG are feasible for delaying the process of renal fibrosis by inhibiting the expression of α-SMA expression and reducing ECM synthesis. It was noteworthy that the combination of EMO and DAG, whether in solution or in liposomal formulations, could significantly reduce the protein levels of Smad3, α-SMA, Col-I, and FN compared to the EMO group ($P < 0.01$), indicating that the combination of EMO and DAG has a synergistic effect on the treatment of renal fibrosis. Interestingly, compared to liposomal formulations, the EMO/DAG solution has shown stronger modulatory effects on fibrosis-related protein levels. This result can be explained by the differences in cellular uptake mechanisms between liposomal formulations and free drugs [51]. Endocytosis is the main method by which liposomes enter the intracellular environment, which is slower than the transmembrane process of free drugs. Furthermore, the sustained release of EMO and DAG from liposomal formulations also contributed to this phenomenon. Hence, we speculate that the expression of these renal fibrosis-related proteins will

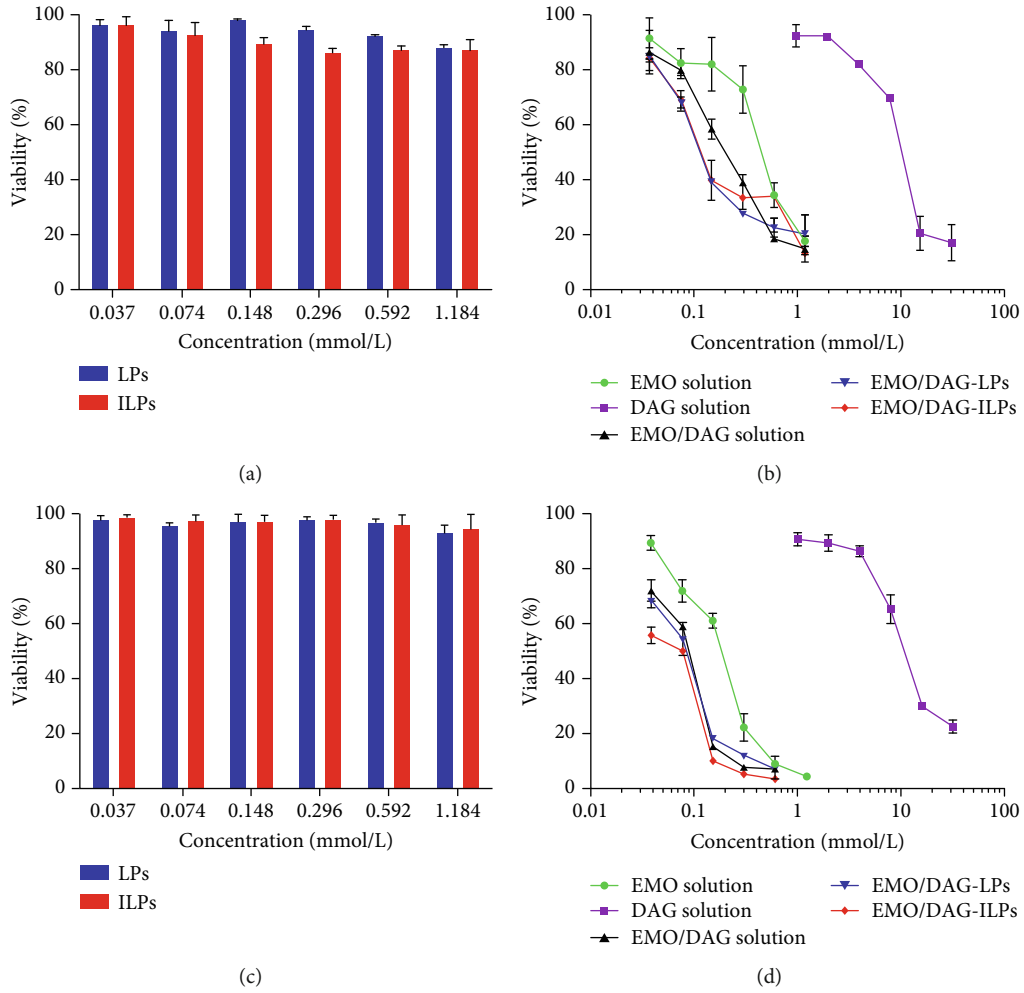

Figure 5: Cell viability of NIH3T3 cells after treatment with blank liposomes (a) and various formulations (b). Cell viability of HBZY-1 cells after treatment with blank liposomes (c) and various formulations (d).

Table 2: IC_{50} values of NIH3T3 and HBZY-1 cells exposed to various formulations.

Group	IC_{50} (mM)	
	NIH3T3	HBZY-1
EMO solution	0.45 ± 0.04	0.16 ± 0.01
DAG solution	9.78 ± 0.5657	11.80 ± 0.65
EMO/DAG solution	0.22 ± 0.01^{aa}	0.14 ± 0.01^{a}
EMO/DAG-LPs	0.15 ± 0.01^{aabb}	0.13 ± 0.01^{aa}
EMO/DAG-ILPs	0.16 ± 0.01^{aabb}	0.11 ± 0.01^{aabc}

∗Data represented as means ± SD and was measured three times ($^{a}P < 0.05$, $^{aa}P < 0.01$, compared to the EMO group; $^{b}P < 0.05$, $^{bb}P < 0.01$, compared to the EMO/DAG group; $^{c}P < 0.05$ compared to the LPs group).

be further tempered by the extension of incubation with liposomal formulations, which are at least as effective as the EMO/DAG solution with regard to its *in vitro* antifibrotic properties [52]. Moreover, the ILPs were superior to LPs in modulating protein levels of Smad3, α-SMA, Col-I, and FN, especially for Col-I. The downregulation effect of LPs and ILPs on α-SMA and FN protein in NIH3T3 cells is superior to that in HBZY-1 cells ($P < 0.05$), except for Smad3 and Col-I ($P > 0.05$). This result may be related to the difference of cell lines.

Changes in renal fibrosis-related proteins in HBZY-1 cells were also evaluated after the cells were treated with different formulations considering the important role that MCs play in kidney fibrosis. As shown in Figure 7, formulations including EMO/DAG solution, EMO solution, EMO/DAG-LPs, and EMO/DAG-ILPs all showed strong suppression of renal fibrosis-related proteins. Note that the combination of EMO and DAG, whether in solutions or in liposomal formulations, had a superior ability to downregulate the Smad3 protein. It is well recognized that Smad3 is the key mediator of TGF-β1-induced ECM production and tissue fibrosis [53, 54].

Furthermore, Figure 7 reflected the stronger inhibitory effect of EMO/DAG-ILPs on Smad3, α-SMA, and Col-I expression compared to EMO/DAG-LPs, which confirmed the effectiveness of anti-alpha8 integrin-modified ILPs by targeting MCs. Collectively, these data indicate that EMO/DAG-ILPs can effectively alleviate renal fibrosis by targeting MCs. We will perform animal experiments in the future to fully confirm the above findings.

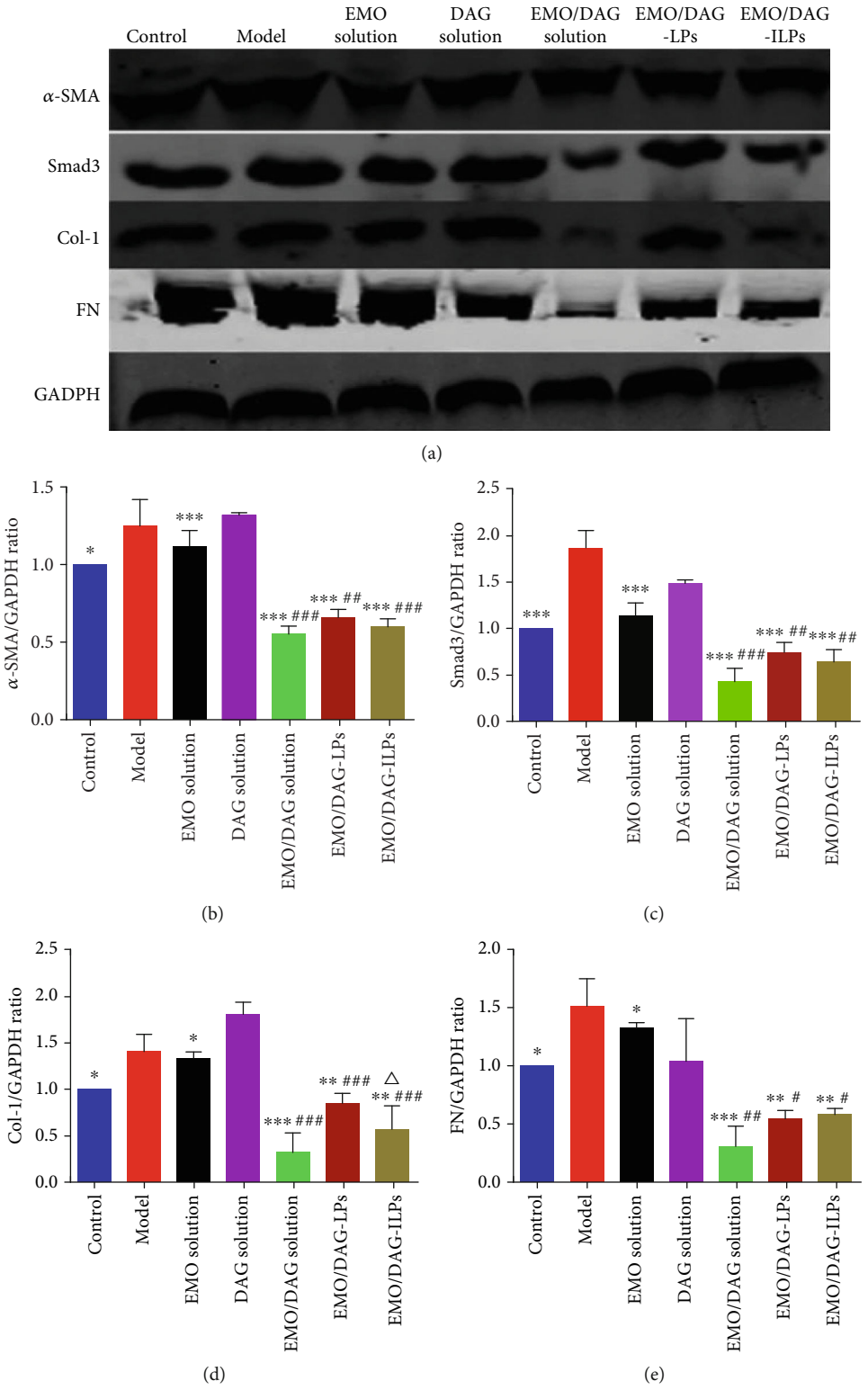

Figure 6: Effects of various formulations on protein levels in NIH3T3 cells. A reprehensive images of renal fibrosis-related proteins (α-SMA, Smad3, Col-I, and FN). (b–e) The relative protein quantification of α-SMA, Smad3, Col-I, and FN in NIH3T3 cells ($*P < 0.05$, $**P < 0.01$, and $***P < 0.001$, compared to the model group. $^{\#}P < 0.05$, $^{\#\#}P < 0.01$, and $^{\#\#\#}P < 0.001$, compared to the EMO solution group).

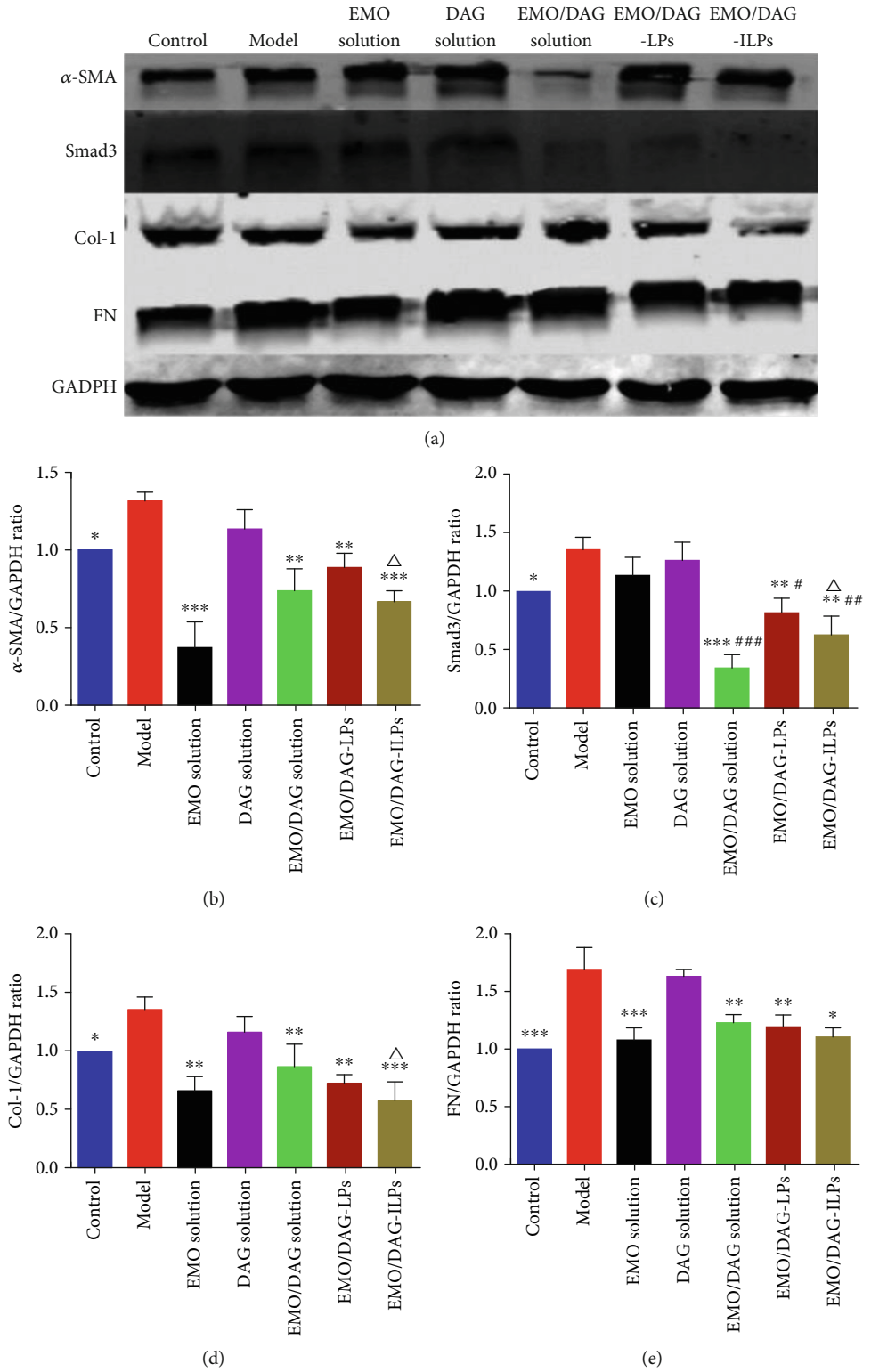

Figure 7: Effects of various formulations on protein expression of HBZY-1 cells. Reprehensive images of renal fibrosis-related proteins (α-SMA, Smad3, Col-I, and FN). (b–e) The relative protein quantification of α-SMA, Smad3, Col-I, and FN in HBZY-1 cells ($*P < 0.05$, $**P < 0.01$, and $*** P < 0.001$, compared to the model group. $^{\#}P < 0.05$, $^{\#\#}P < 0.01$, and $^{\#\#\#}P < 0.001$, compared to the EMO solution group, $^{\triangle}P < 0.05$ and $^{\triangle\triangle}P < 0.01$, compared to the EMO/DAG-LPs group).

4. Conclusion

We have successfully designed and characterized EMO/DAG coloaded anti-alpha8 integrin-conjugated immunoliposomes for targeted delivery and combined therapy. The coloaded immunoliposomes presented nanometric particle size, high drug entrapment, and sufficient conjugation efficiency. *In vitro* drug release demonstrated that the molar ratio of the released agents was within the synergy range after a small burst release of DAG. Cells with a high level of alpha8 integrin expression showed better cellular uptake of immunoliposomes and higher cell growth inhibition. Moreover, the combination of EMO and DAG can inhibit the expression of renal fibrosis-related proteins (α-SMA, Smad3, Col-I, and FN), thereby delaying the progress of renal fibrosis. Based on the promising results of *in vitro* studies, we anticipate that the EMO/DAG-loaded immunoliposomes will prove to be an efficient delivery system for the treatment of renal fibrosis *in vivo*.

Data Availability

On data availability statement, the raw/processed data required to reproduce these findings cannot be shared at this time as the data also forms part of an ongoing study.

Conflicts of Interest

No potential conflict of interest was reported by authors.

Acknowledgments

This work was supported by the National Science Foundation of China (No. 81873018 and 81373982).

Supplementary Materials

Figure S1: cell viability of NIH3T3 cells after treatment with various formulations. Figure S2: the IC50 values (A) and combination index (CI) (B) in NIH3T3 cells of various formulations ($*P < 0.05$, $**P < 0.01$, and $***P < 0.001$ compared to the EMO solution group). Figure S3: the expression of α-SMA protein in NIH3T3 cells induced by TGF-β1 (5 ng/mL) ($*P < 0.05$, compared to the control group). Figure S4: effects of various formulations on protein levels in NIH3T3 cells. Reprehensive images of renal fibrosis-related proteins (α-SMA, TGF-β1, Col-I, and FN). (B–E) The relative protein quantification of α-SMA, TGF-β1, Col-I, and FN in NIH3T3 cells, respectively ($*P < 0.05$, $**P < 0.01$, and $***P < 0.001$, compared to the control group. $^{\#}P < 0.05$ and $^{\#\#}P < 0.01$, compared to the EMO solution group). *(Supplementary Materials)*

References

[1] B. Bikbov, N. Perico, and G. Remuzzi, "Disparities in chronic kidney disease prevalence among males and females in 195 countries: analysis of the Global Burden of Disease 2016 Study," *Nephron*, vol. 139, no. 4, pp. 313–318, 2018.

[2] A. C. Webster, E. V. Nagler, R. L. Morton, and P. Masson, "Chronic kidney disease," *Lancet*, vol. 389, no. 10075, pp. 1238–1252, 2017.

[3] P. Boor, T. Ostendorf, and J. Floege, "Renal fibrosis: novel insights into mechanisms and therapeutic targets," *Nature Reviews. Nephrology*, vol. 6, no. 11, pp. 643–656, 2010.

[4] S. Meran and R. Steadman, "Fibroblasts and myofibroblasts in renal fibrosis," *International Journal of Experimental Pathology*, vol. 92, no. 3, pp. 158–167, 2011.

[5] H. Kurihara and T. Sakai, "Cell biology of mesangial cells: the third cell that maintains the glomerular capillary," *Anatomical Science International*, vol. 92, no. 2, pp. 173–186, 2017.

[6] M. V. Nastase, J. Zeng-Brouwers, M. Wygrecka, and L. Schaefer, "Targeting renal fibrosis: mechanisms and drug delivery systems," *Advanced Drug Delivery Reviews*, vol. 129, pp. 295–307, 2018.

[7] G. Vega, S. Alarcón, and M. R. San, "The cellular and signalling alterations conducted by TGF-β contributing to renal fibrosis," *Cytokine*, vol. 88, pp. 115–125, 2016.

[8] I. Marek, R. Becker, F. B. Fahlbusch et al., "Expression of the Alpha8 integrin chain facilitates phagocytosis by renal mesangial cells," *Cellular Physiology and Biochemistry*, vol. 45, no. 6, pp. 2161–2173, 2018.

[9] I. Marek, G. Volkert, A. Jahn et al., "Lack of α8 integrin leads to morphological changes in renal mesangial cells, but not in vascular smooth muscle cells," *BMC Cell Biology*, vol. 11, no. 1, p. 102, 2010.

[10] M. E. Ougaard, H. E. Jensen, I. D. Thuen, E. G. Petersen, and P. H. Kvist, "Inhibitors of the renin-angiotensin system ameliorates clinical and pathological aspects of experimentally induced nephrotoxic serum nephritis," *Renal Failure*, vol. 40, no. 1, pp. 640–648, 2018.

[11] X. Dong, J. Fu, X. Yin et al., "Emodin: a review of its pharmacology, toxicity and pharmacokinetics," *Phytotherapy Research*, vol. 30, no. 8, pp. 1207–1218, 2016.

[12] M. Wang, R. Zhao, W. Wang, X. Mao, and J. Yu, "Lipid regulation effects of Polygoni Multiflori Radix, its processed products and its major substances on steatosis human liver cell line L02," *Journal of Ethnopharmacology*, vol. 139, no. 1, pp. 287–293, 2012.

[13] M. H. Lee, L. Kao, and C. C. Lin, "Comparison of the antioxidant and transmembrane permeative activities of the different Polygonum cuspidatum extracts in phospholipid-based microemulsions," *Journal of Agricultural and Food Chemistry*, vol. 59, no. 17, pp. 9135–9141, 2011.

[14] Z. Xiang, H. Sun, X. Cai, D. Chen, and X. Zheng, "The study on the material basis and the mechanism for anti-renal interstitial fibrosis efficacy of rhubarb through integration of metabonomics and network pharmacology," *Molecular BioSystems*, vol. 11, no. 4, pp. 1067–1078, 2015.

[15] L. Ma, H. Li, S. Zhang et al., "Emodin ameliorates renal fibrosis in rats via TGF-β1/Smad signaling pathway and function study of Smurf 2," *International Urology and Nephrology*, vol. 50, no. 2, pp. 373–382, 2018.

[16] D. Jing, H. Bai, and S. Yin, "Renoprotective effects of emodin against diabetic nephropathy in rat models are mediated via PI3K/Akt/GSK-3β and Bax/caspase-3 signaling pathways," *Experimental and Therapeutic Medicine*, vol. 14, no. 5, pp. 5163–5169, 2017.

[17] C. S. Shia, Y. C. Hou, S. Y. Tsai, P. H. Huieh, Y. L. Leu, and P. D. Chao, "Differences in pharmacokinetics and ex vivo

antioxidant activity following intravenous and oral administrations of emodin to rats," *Journal of Pharmaceutical Sciences*, vol. 99, no. 4, pp. 2185–2195, 2010.

[18] M. N. Asl and H. Hosseinzadeh, "Review of pharmacological effects of Glycyrrhiza sp. and its bioactive compounds," *Phytotherapy Research*, vol. 22, no. 6, pp. 709–724, 2008.

[19] Y. Zhou, X. Tong, S. Ren et al., "Synergistic anti-liver fibrosis actions of total astragalus saponins and glycyrrhizic acid via TGF-β1/Smads signaling pathway modulation," *Journal of Ethnopharmacology*, vol. 190, pp. 83–90, 2016.

[20] W. Y. Cai, Y. Y. Gu, A. M. Li, H. Q. Cui, and Y. Yao, "Effect of alprostadil combined with Diammonium glycyrrhizinate on renal interstitial fibrosis in SD rats," *Asian Pacific Journal of Tropical Medicine*, vol. 7, no. 11, pp. 900–904, 2014.

[21] W. Arjumand and S. Sultana, "Glycyrrhizic acid: a phytochemical with a protective role against cisplatin-induced genotoxicity and nephrotoxicity," *Life Sciences*, vol. 89, no. 13-14, pp. 422–429, 2011.

[22] E. Yamamoto, "In vitro release method for liposome drug products," *Yakugaku Zasshi*, vol. 139, no. 2, pp. 249–254, 2019.

[23] C. P. Liu, Y. Hu, J. C. Lin, H. L. Fu, L. Y. Lim, and Z. X. Yuan, "Targeting strategies for drug delivery to the kidney: from renal glomeruli to tubules," *Medicinal Research Reviews*, vol. 39, no. 2, pp. 561–578, 2019.

[24] M. Li, C. Du, N. Guo et al., "Composition design and medical application of liposomes," *European Journal of Medicinal Chemistry*, vol. 164, pp. 640–653, 2019.

[25] D. Ren, J. Luo, Y. Li et al., "Saikosaponin B2 attenuates kidney fibrosis via inhibiting the hedgehog pathway," *Phytomedicine*, vol. 67, p. 153163, 2020.

[26] F. Poosti, R. Bansal, S. Yazdani et al., "Selective delivery of IFN-γ to renal interstitial myofibroblasts: a novel strategy for the treatment of renal fibrosis," *The FASEB Journal*, vol. 29, no. 3, pp. 1029–1042, 2015.

[27] J. Tang, X. Jiang, Y. Zhou, and Y. Dai, "Effects of A2BR on the biological behavior of mouse renal fibroblasts during hypoxia," *Molecular Medicine Reports*, vol. 11, no. 6, pp. 4397–4402, 2015.

[28] J. O. Eloy, R. Petrilli, D. L. Chesca, F. P. Saggioro, R. J. Lee, and J. M. Marchetti, "Anti-HER2 immunoliposomes for co-delivery of paclitaxel and rapamycin for breast cancer therapy," *European Journal of Pharmaceutics and Biopharmaceutics*, vol. 115, pp. 159–167, 2017.

[29] J. Wang, Z. Wu, G. Pan et al., "Enhanced doxorubicin delivery to hepatocellular carcinoma cells via CD147 antibody-conjugated immunoliposomes," *Nanomedicine*, vol. 14, no. 6, pp. 1949–1961, 2018.

[30] S. Gholizadeh, G. R. R. Visweswaran, G. Storm, W. E. Hennink, J. A. A. M. Kamps, and R. J. Kok, "E-selectin targeted immunoliposomes for rapamycin delivery to activated endothelial cells," *International Journal of Pharmaceutics*, vol. 548, no. 2, pp. 759–770, 2018.

[31] Y. Zhou, D. C. Drummond, H. Zou et al., "Impact of single-chain Fv antibody fragment affinity on nanoparticle targeting of epidermal growth factor receptor-expressing tumor cells," *Journal of Molecular Biology*, vol. 371, no. 4, pp. 934–947, 2007.

[32] Y. Wang, F. Liu, Q. Wang et al., "A novel immunoliposome mediated by CD123 antibody targeting to acute myeloid leukemia cells," *International Journal of Pharmaceutics*, vol. 529, no. 1-2, pp. 531–542, 2017.

[33] M. J. Lim, J. Ahn, J. Y. Yi et al., "Induction of galectin-1 by TGF-β1 accelerates fibrosis through enhancing nuclear retention of Smad2," *Experimental Cell Research*, vol. 326, no. 1, pp. 125–135, 2014.

[34] M. Merino, S. Zalba, and M. J. Garrido, "Immunoliposomes in clinical oncology: state of the art and future perspectives," *Journal of Controlled Release*, vol. 275, pp. 162–176, 2018.

[35] P. Sapra and T. M. Allen, "Ligand-targeted liposomal anticancer drugs," *Progress in Lipid Research*, vol. 42, no. 5, pp. 439–462, 2003.

[36] S. B. Kulkarni, G. V. Betageri, and M. Singh, "Factors affecting microencapsulation of drugs in liposomes," *Journal of Microencapsulation*, vol. 12, no. 3, pp. 229–246, 2008.

[37] A. S. Manjappa, P. N. Goel, R. P. Gude, and R. S. Ramachandra Murthy, "Anti-neuropilin 1 antibody Fab' fragment conjugated liposomal docetaxel for active targeting of tumours," *Journal of Drug Targeting*, vol. 22, no. 8, pp. 698–711, 2014.

[38] R. Devi, A. Jain, P. Hurkat, and S. K. Jain, "Dual drug delivery using lactic acid conjugated SLN for effective management of neurocysticercosis," *Pharmaceutical Research*, vol. 32, no. 10, pp. 3137–3148, 2015.

[39] M. J. Peres-Filho, A. P. dos Santos, T. L. Nascimento et al., "Antiproliferative activity and VEGF expression reduction in MCF7 and PC-3 cancer cells by paclitaxel and imatinib co-encapsulation in folate-targeted liposomes," *AAPS PharmSciTech*, vol. 19, no. 1, pp. 201–212, 2018.

[40] H. T. Phan and A. J. Haes, "What does nanoparticle stability mean?," *The Journal of Physical Chemistry. C, Nanomaterials and Interfaces*, vol. 123, no. 27, pp. 16495–16507, 2019.

[41] T. L. Moore, L. Rodriguez-Lorenzo, V. Hirsch et al., "Nanoparticle colloidal stability in cell culture media and impact on cellular interactions," *Chemical Society Reviews*, vol. 44, no. 17, pp. 6287–6305, 2015.

[42] E. Alipour, D. Halverson, S. McWhirter, and G. C. Walker, "Phospholipid bilayers: stability and encapsulation of nanoparticles," *Annual Review of Physical Chemistry*, vol. 68, no. 1, pp. 261–283, 2017.

[43] G. Lu, T. Z. Forbes, and A. J. Haes, "SERS detection of uranyl using functionalized gold nanostars promoted by nanoparticle shape and size," *The Analyst*, vol. 141, no. 17, pp. 5137–5143, 2016.

[44] M. Stolzoff, I. Ekladious, A. H. Colby, Y. L. Colson, T. M. Porter, and M. W. Grinstaff, "Synthesis and characterization of hybrid polymer/lipid expansile nanoparticles: imparting surface functionality for targeting and stability," *Biomacromolecules*, vol. 16, no. 7, pp. 1958–1966, 2015.

[45] M. C. Smith, R. M. Crist, J. D. Clogston, and S. E. McNeil, "Zeta potential: a case study of cationic, anionic, and neutral liposomes," *Analytical and Bioanalytical Chemistry*, vol. 409, no. 24, pp. 5779–5787, 2017.

[46] B. Liang, M. Shahbaz, Y. Wang et al., "Integrinβ6-targeted immunoliposomes mediate tumor-specific drug delivery and enhance therapeutic efficacy in colon carcinoma," *Clinical Cancer Research*, vol. 21, no. 5, pp. 1183–1195, 2015.

[47] J. W. Liang, S. L. Hsiu, P. P. Wu, and P. D. Chao, "Emodin pharmacokinetics in rabbits," *Planta Medica*, vol. 61, no. 5, pp. 406–408, 1995.

[48] Y. Scindia, U. Deshmukh, P. R. Thimmalapura, and H. Bagavant, "Anti-alpha8 integrin immunoliposomes in glomeruli of lupus-susceptible mice: a novel system for delivery of therapeutic agents to the renal glomerulus in systemic lupus

erythematosus," *Arthritis and Rheumatism*, vol. 58, no. 12, pp. 3884–3891, 2008.

[49] H. H. Hu, D. Q. Chen, Y. N. Wang et al., "New insights into TGF-β/Smad signaling in tissue fibrosis," *Chemico-Biological Interactions*, vol. 292, pp. 76–83, 2018.

[50] L. Chen, T. Yang, D. W. Lu et al., "Central role of dysregulation of TGF-β/Smad in CKD progression and potential targets of its treatment," *Biomedicine & Pharmacotherapy*, vol. 101, pp. 670–681, 2018.

[51] K. B. Johnsen, A. Burkhart, F. Melander et al., "Targeting transferrin receptors at the blood-brain barrier improves the uptake of immunoliposomes and subsequent cargo transport into the brain parenchyma," *Scientific Reports*, vol. 7, no. 1, p. 10396, 2017.

[52] S. Yang, "Preparation, in vitro characterization and pharmacokinetic study of coenzyme Q10 long-circulating liposomes," *Drug research*, vol. 68, no. 5, pp. 270–279, 2018.

[53] F. Verrecchia, L. Vindevoghel, R. J. Lechleider, J. Uitto, A. B. Roberts, and A. Mauviel, "Smad3/AP-1 interactions control transcriptional responses to TGF-beta in a promoter-specific manner," *Oncogene*, vol. 20, no. 26, pp. 3332–3340, 2001.

[54] L. Vindevoghel, R. J. Lechleider, A. Kon et al., "SMAD3/4-dependent transcriptional activation of the human type VII collagen gene (COL7A1) promoter by transforming growth factor beta," *Proceedings of the National Academy of Sciences of the United States of America*, vol. 95, no. 25, pp. 14769–14774, 1998.